

OPTOMECHANICS

Cooling of a levitated nanoparticle to the motional quantum ground state

Uroš Delić^{1,2*}, Manuel Reisenbauer¹, Kahan Dare^{1,2}, David Grass^{1,†}, Vladan Vuletić³, Nikolai Kiesel¹, Markus Aspelmeyer^{1,2*}

Quantum control of complex objects in the regime of large size and mass provides opportunities for sensing applications and tests of fundamental physics. The realization of such extreme quantum states of matter remains a major challenge. We demonstrate a quantum interface that combines optical trapping of solids with cavity-mediated light-matter interaction. Precise control over the frequency and position of the trap laser with respect to the optical cavity allowed us to laser-cool an optically trapped nanoparticle into its quantum ground state of motion from room temperature. The particle comprises 10^8 atoms, similar to current Bose-Einstein condensates, with the density of a solid object. Our cooling technique, in combination with optical trap manipulation, may enable otherwise unachievable superposition states involving large masses.

Optical levitation of dielectric particles works by using forces induced by laser light that are strong enough to overcome gravity. At its most fundamental level, an incoming laser polarizes the dielectric material, which in turn interacts with the radiation field of the laser. As a consequence, a particle in a tightly focused laser beam experiences a gradient force toward the intensity maximum of the beam, resulting in a three-dimensional confinement of the particle (*1*). Such “optical tweezers” have become a powerful tool to manipulate dielectric objects in isolation from other environments.

In the domain of quantum physics, optical trapping and cooling of atoms has enabled the study of individual atoms and quantum gases. It is also a fundamental technique for confining particles to optical lattice geometries for the study of many-body quantum phenomena. As such, laser cooling techniques should enable the preparation of a levitated solid-state particle in its quantum ground state of motion (*2–4*). The particle wave packet can then be expanded and modified by a sequence of free fall, coherent manipulations, and quantum measurement operations (*5*). This provides a promising platform for exploring macroscopic quantum phenomena. It entails the ability to manipulate the spatial profile of the trapping laser for implementing nonlinear potentials, and may open the possibility of creating nonclassical states of motion such as non-Gaussian states or large spatial superpositions. This is

in stark contrast to experiments that prepare motional quantum states using solid-state harmonic oscillators, where coupling to external nonlinear systems or measurements provides the interaction for nonclassical state preparation (*6–8*). Unlike ultracold quantum gases, motional quantum states of trapped solids involve the collective motion of all atoms and hence provide a natural way toward spatial superpositions of large mass differences in so-called Schrödinger cat states, which is a fundamentally hard task for gaseous systems (*9*).

A key requirement for entering this new regime is to prepare the particle wave packet in a sufficiently pure quantum state—in this case, to cool its motion into the quantum ground state. One possibility is to monitor the particle motion with a sensitivity at or below the ground-state size of the wave packet and apply a feedback force to directly counteract the motion. Such feedback cooling to the quantum ground state has recently been demonstrated for harmonic modes of cryogenically cooled micromechanical membranes (*10*). In the context of levitated nanoparticles, feedback cooling was initially introduced to provide stable levitation in high vacuum. At present, feedback cooling is limited to approximately four motional quanta (phonons) (*11*). A different approach is derived from the laser cooling of atoms, where the absorption and re-emission of Doppler-shifted laser photons provides a velocity-dependent scattering force. The presence of an optical cavity modifies the electromagnetic boundary conditions for the scattered light. We can use this to tailor the scattering rates and therefore cool particles without an accessible internal level structure, such as molecules or dielectric solids (*12, 13*). These cavity-cooling schemes have been used in the past to achieve ground-state cooling of various systems ranging from individual atoms to cryogenically cooled modes of solid-

state nano- and micromechanical oscillators in the context of cavity optomechanics (*14*). Previous attempts to apply cavity cooling to levitated solids have proven challenging, and cooling was limited to several hundred phonons (*15–18*), mainly as a result of co-trapping associated with high intracavity photon number and excessive laser phase noise heating at low motional frequencies (<1 MHz) (*17, 18*). We apply a modified scheme—cavity cooling by coherent scattering (*19–21*)—that circumvents these shortcomings and enables direct ground-state cooling of a solid in a room-temperature environment.

In our experimental setup, we trap a spherical silica particle inside a vacuum chamber using an optical tweezer. A tightly focused laser beam (power in the focus $P_{\text{tw}} \approx 400$ mW, wavelength $\lambda = 1064$ nm, and frequency $\omega_{\text{tw}} = 2\pi c/\lambda$, where c is the speed of light in vacuum) creates a three-dimensional harmonic potential for the particle motion with motional frequencies $(\Omega_x, \Omega_y, \Omega_z)/2\pi \approx (305, 275, 80)$ kHz. We position the particle within an optical cavity (cavity finesse $\mathcal{F} \approx 73,000$; cavity linewidth $\kappa/2\pi = 193 \pm 4$ kHz; cavity frequency $\omega_{\text{cav}} = \omega_{\text{tw}} + \Delta$, where Δ is the laser detuning), which collects the tweezer light scattered off the nanoparticle under approximately a right angle (Fig. 1A). The particle has subwavelength dimension and hence resembles, to a good approximation, a dipole emitter. When driven by the optical tweezer, the particle coherently scatters dipole radiation predominantly orthogonal to the tweezer polarization axis. Motorized translation stages in the tweezer optics allow us to position the particle with an accuracy of a few nanometers with respect to the cavity axis (x -direction) such that the particle can be well localized within one period of the cavity standing wave field. To achieve optimal cooling along the cavity axis, the particle needs to be located at an intensity minimum of the cavity standing wave field (*19, 20*). At that location the particle is “dark,” and accordingly all dipole scattering into the cavity mode is inhibited because of destructive interference imposed by the cavity. The particle motion breaks this symmetry, and therefore only inelastically scattered Stokes- and anti-Stokes photons at sideband frequencies $\omega_{\text{tw}} \pm \Omega_x$ can propagate in the cavity.

Cavity cooling of the particle motion occurs because Stokes scattering processes along the cavity, which increase the kinetic energy of the particle by $\hbar\Omega_x$ per photon, are suppressed, while anti-Stokes scattering processes, which reduce the energy accordingly, are enhanced (*14*). This process is maximized at the optimal detuning $\Delta \approx \Omega_x$, where the anti-Stokes sideband becomes fully resonant with the cavity. A particle in its quantum ground state of motion cannot further reduce its energy, hence anti-Stokes scattering close to the ground state is fundamentally inhibited (Fig. 1, B and C). The

¹Vienna Center for Quantum Science and Technology, Faculty of Physics, University of Vienna, A-1090 Vienna, Austria. ²Institute for Quantum Optics and Quantum Information, Austrian Academy of Sciences, A-1090 Vienna, Austria. ³Department of Physics and Research Laboratory of Electronics, Massachusetts Institute of Technology, Cambridge, MA 02139, USA.

*Corresponding author. Email: uros.delic@univie.ac.at (U.D.); markus.aspelmeyer@univie.ac.at (M.A.)
[†]Present address: Department of Chemistry, Duke University, Durham, NC 27708, USA.

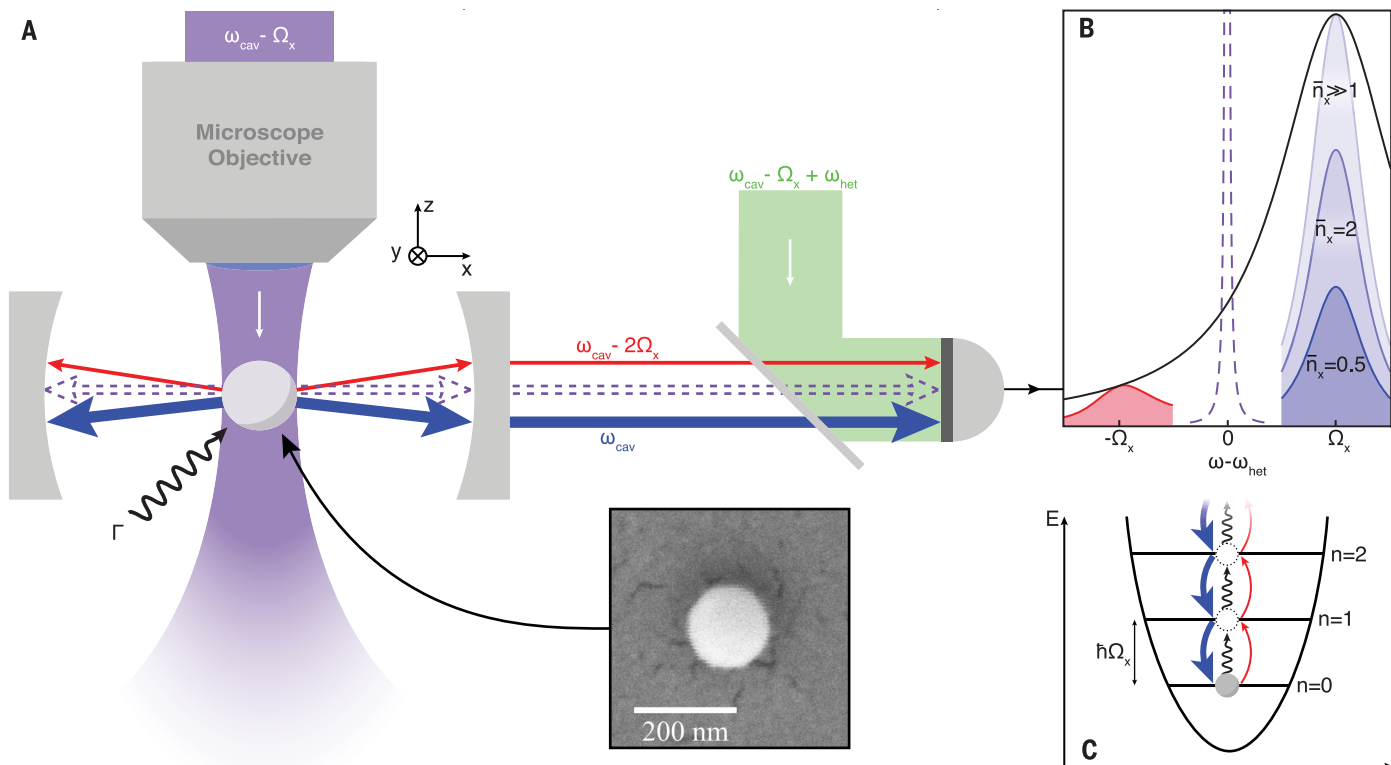


Fig. 1. Cavity cooling and sideband thermometry. (A) A silica nanoparticle of nominal diameter $d = 143 \pm 4$ nm (SEM image) is trapped in an optical tweezer (purple). The frequency of the tweezer laser ω_{tw} is detuned from the initially empty cavity resonance ω_{cav} such that $\omega_{\text{tw}} = \omega_{\text{cav}} - \Omega_x$. Scattering of the tweezer light into the optical cavity is maximized via the tweezer polarization. The spatial mode overlap between the dipole emission pattern of the silica nanoparticle and the optical cavity mode results in a Purcell enhancement of the scattered radiation by a factor of 8 relative to a free-space configuration. When the particle is positioned at a cavity node, the elastic scattering of the tweezer light (dashed purple arrows) is suppressed, leaving only the inelastically scattered Stokes (red) and anti-Stokes (blue) sidebands at frequencies $\omega_{\text{cav}} - 2\Omega_x$ and ω_{cav} , respectively. Mixing the scattered sidebands with a strong local oscillator (green) at $\omega_{\text{LO}} = \omega_{\text{tw}} + \omega_{\text{het}}$ allows us to separately detect both sidebands in a

heterodyne measurement at the cavity output port. The total heating rate from the environment is represented here as Γ . (B) Heterodyne measurement of the Stokes and anti-Stokes sidebands. The phonon occupation affects the overall scattering rates, which are initially modified by the cavity response (black). For large phonon occupations ($\bar{n}_x \gg 1$), the relative amplitudes of the Stokes and anti-Stokes sidebands are completely described by the cavity transmission function. As the nanoparticle approaches the motional ground state, the sideband ratio is modified because the oscillator cannot undergo an anti-Stokes scattering process. This asymmetry allows for direct thermometry of the phonon occupation. The suppressed elastic scattering contribution is depicted in dashed purple for reference. (C) Depiction of the phonon energy levels close to the ground state. The heating rate from the environment and the Stokes scattering rate are balanced by the anti-Stokes scattering rate.

resulting sideband asymmetry in the scattering rates is a direct measure of the temperature of the harmonic particle motion, which does not require calibration to a reference bath (22). We observe these sidebands, which are modulated by the cavity envelope (23), using frequency-selective heterodyne detection of the cavity output, specifically by mixing it with a strong local oscillator field ($P_{\text{L.O}} \approx 400$ μW) detuned from the tweezer laser by $\omega_{\text{het}}/2\pi = 10.2$ MHz.

Independent measurements of the cavity linewidth κ and the laser detuning Δ allow us to correct the detected sideband ratios for the cavity envelope (24), and hence to extract the motional temperature of the particle via the fundamental sideband asymmetry (Fig. 2A). For this method to work reliably, it is important to exclude all relevant influences of noise contributions to the sideband asymmetry (25). We ensure this by confirming that the detec-

tion process is shot noise-limited and that both amplitude- and phase-noise contributions of the drive laser are negligible (24). Figure 2B shows the measured phonon number \bar{n}_x along the cavity axis for different laser detunings Δ . For near-optimal detuning of $\Delta/2\pi = 315$ kHz, we observe a final occupation as low as $\bar{n}_x = 0.43 \pm 0.03$, corresponding to a temperature of 12.2 ± 0.5 μK and a ground-state probability of $70 \pm 2\%$. Note that in contrast to previous quantum experiments involving cryogenically cooled solid-state oscillators, ground-state cooling here is achieved in a room-temperature environment.

The final occupation \bar{n}_{fin} along any direction is reached when the total heating rate Γ_x is balanced by the cooling rate $\bar{n}_{\text{fin}} \times \gamma$, where γ is the linewidth of the motional sidebands (26). For the resolved sideband regime ($\kappa < \Omega_x$) as studied here, and in the absence of any other

heating mechanisms, Stokes scattering due to the finite cavity linewidth limits cooling with optimal parameters to a minimum phonon occupation of $\bar{n}_{\text{min}} = (\kappa/4\Omega_x)^2 \approx 0.025$. Note that in this case, detailed balance implies that the fundamental ground-state asymmetry exactly compensates the effect of the cavity envelope and therefore both sidebands have equal power. Additional sources of heating are balanced by larger anti-Stokes scattering, which results in the overall observed sideband imbalance. By independently measuring \bar{n}_x and γ , we extract a total heating rate as low as $\Gamma_x/2\pi = 20.6 \pm 2.3$ kHz at a pressure of $\sim 10^{-6}$ mbar. This is consistent with the separately measured heating rate due to background gas collisions (18), $\Gamma_{\text{gas}}/2\pi = 16.1 \pm 1.2$ kHz, and the expected heating contributions from photon recoil, $\Gamma_{\text{rec}}/2\pi \approx 6$ kHz, and from laser phase noise, $\Gamma_{\text{phase}}/2\pi < 200$ Hz (24).

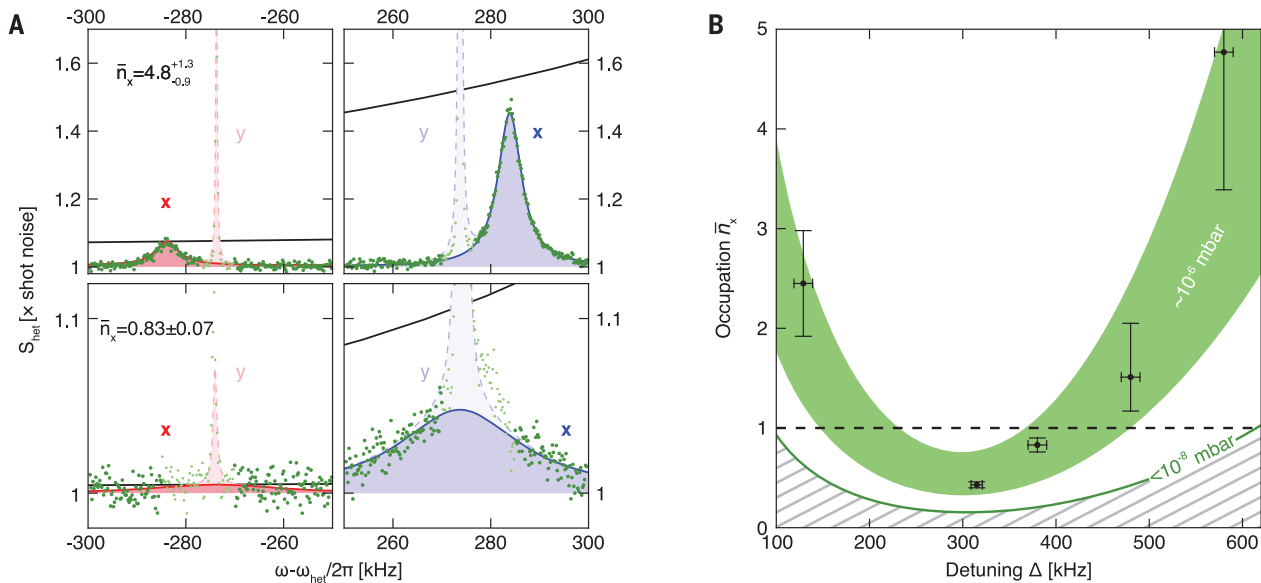


Fig. 2. Thermometry of the phonon occupation associated with the cavity axial motion. (A) Heterodyne spectra. Shown are the sideband power spectra for Stokes (left) and anti-Stokes (right) scattering for different detunings $\Delta/2\pi = 580 \pm 10$ kHz (top row) and $\Delta/2\pi = 380 \pm 10$ kHz (bottom row). Red and blue solid lines are fits to the data representing the x motion. Also shown are lighter red and blue dashed lines, which are part of the fitted spectrum corresponding to the y motion at $\Omega_y/2\pi = 275 \pm 1$ kHz. Black solid line indicates the cavity transmission function normalized to the Stokes sideband power. Smaller temperatures show a stronger deviation of the anti-Stokes scattered sideband power from the cavity envelope, as described in the text. The ratio of amplitudes together with the independently measured cavity

transmission function yields the final occupation \bar{n}_x . (B) Occupation \bar{n}_x as a function of tweezer laser detuning. The cooling rate is maximal when the optical tweezer is detuned from the cavity resonance by approximately the motional frequency $\Delta/2\pi \approx 315$ kHz. At this maximal cooling point, we achieve a phonon occupation of $\bar{n}_x = 0.43 \pm 0.03$. Error bars take into account the experimental uncertainty of the laser detuning and the cavity decay rate in combination with the errors inherent to the fit. The wide green band is a theoretical model based on system parameters, which takes into account pressure drifts during the measurement. The lower dark green line corresponds to the expected occupation when the environment pressure is below 10^{-8} mbar, at which heating due to collisions with the background gas becomes negligible relative to recoil heating.

In future experiments, reduction of decoherence can be achieved mainly by lower background pressures, but potentially also by operating at lower temperatures and using smaller cavity mode volumes. At present, using the measured heating rates, we estimate a maximum coherence time of $7.6 \pm 1 \mu\text{s}$ in the optical trap, corresponding to approximately 15 coherent oscillations before populating the ground state with one phonon (2, 27). In a free-fall experiment, where the particle would be released from the optical trap, the dominant source for decoherence is the collision with background gas molecules. At the achieved pressure of 10^{-6} mbar, this limits the free-fall coherence time to $1.4 \mu\text{s}$, which would allow for an expansion of the wave packet by approximately a factor of 3, from the ground state size of 3.1 pm to 10.2 pm (24, 28). Larger wave packet sizes can be achieved by further decreasing this decoherence rate—for example, by operating at much lower pressures. Blackbody radiation will then become the dominant source of decoherence and will, for our room-temperature parameters, allow for wave packet expansions up to several nanometers. A wave packet size on the order of the particle radius could be achieved by combining ultrahigh vacuum (approximately 10^{-11} mbar) with cryogenic temperatures (below 130 K).

The combination of cavity optomechanical quantum control of levitated systems and free-fall experiments can open up a new regime of macro-quantum physics, with additional potential applications in quantum sensing (29) and other fields of fundamental physics (30). Most important, we believe that the quantum control of levitated systems is a viable route toward experiments in which quantum systems can act as gravitational source masses, as was originally suggested by Feynman (31) and recently revisited in the context of levitation (32, 33).

REFERENCES AND NOTES

1. A. Ashkin, J. M. Dziedzic, J. E. Bjorkholm, S. Chu, *Opt. Lett.* **11**, 288 (1986).
2. D. E. Chang *et al.*, *Proc. Natl. Acad. Sci. U.S.A.* **107**, 1005–1010 (2010).
3. O. Romero-Isart, M. L. Juan, R. Quidant, J. I. Cirac, *New J. Phys.* **12**, 033015 (2010).
4. P. F. Barker, M. N. Schneider, *Phys. Rev. A* **81**, 023826 (2010).
5. O. Romero-Isart *et al.*, *Phys. Rev. Lett.* **107**, 020405 (2011).
6. A. D. O’Connell *et al.*, *Nature* **464**, 697–703 (2010).
7. Y. Chu *et al.*, *Nature* **563**, 666–670 (2018).
8. R. Riedinger *et al.*, *Nature* **530**, 313–316 (2016).
9. J. I. Cirac, M. Lewenstein, K. Molmer, P. Zoller, *Phys. Rev. A* **57**, 1208–1218 (1998).
10. M. Rossi, D. Mason, J. Chen, Y. Tsaturyan, A. Schliesser, *Nature* **563**, 53–58 (2018).
11. F. Tebbenjohanns, M. Frimmer, V. Jain, D. Windey, L. Novotny, *Phys. Rev. Lett.* **124**, 013603 (2020).
12. P. Horak, G. Hechenblaikner, K. M. Gheri, H. Stecher, H. Ritsch, *Phys. Rev. Lett.* **79**, 4974–4977 (1997).
13. V. Vuletić, S. Chu, *Phys. Rev. Lett.* **84**, 3787–3790 (2000).
14. M. Aspelmeyer, T. J. Kippenberg, F. Marquardt, *Rev. Mod. Phys.* **86**, 1391–1452 (2014).

15. N. Kiesel *et al.*, *Proc. Natl. Acad. Sci. U.S.A.* **110**, 14180–14185 (2013).
16. J. Millen, P. Z. G. Fonseca, T. Mavrogordatos, T. S. Monteiro, P. F. Barker, *Phys. Rev. Lett.* **114**, 123602 (2015).
17. N. Meyer *et al.*, *Phys. Rev. Lett.* **123**, 153601 (2019).
18. U. Delić *et al.*, arXiv 1902.06605 [physics.optics] (18 February 2019).
19. U. Delić *et al.*, *Phys. Rev. Lett.* **122**, 123602 (2019).
20. D. Windey *et al.*, *Phys. Rev. Lett.* **122**, 123601 (2019).
21. S. Nimmrichter, K. Hammerer, P. Asenbaum, H. Ritsch, M. Arndt, *New J. Phys.* **12**, 083003 (2010).
22. A. H. Safavi-Naeini *et al.*, *Phys. Rev. Lett.* **108**, 033602 (2012).
23. R. W. Peterson *et al.*, *Phys. Rev. Lett.* **116**, 063601 (2016).
24. See supplementary materials.
25. V. Sudhir *et al.*, *Phys. Rev. X* **7**, 011001 (2017).
26. V. Jain *et al.*, *Phys. Rev. Lett.* **116**, 243601 (2016).
27. O. Romero-Isart *et al.*, *Phys. Rev. A* **83**, 013803 (2011).
28. O. Romero-Isart, *Phys. Rev. A* **84**, 052121 (2011).
29. A. A. Geraci, S. B. Papp, J. Kitching, *Phys. Rev. Lett.* **105**, 101101 (2010).
30. J. Bateman, I. McHardy, A. Merle, T. R. Morris, H. Ulbricht, *Sci. Rep.* **5**, 8058 (2015).
31. D. Rickles, C. M. DeWitt, *The Role of Gravitation in Physics: Report from the 1957 Chapel Hill Conference* (2011); <https://edition-open-sources.org/media/sources/5/Sources5.pdf>.
32. S. Bose *et al.*, *Phys. Rev. Lett.* **119**, 240401 (2017).
33. C. Marletto, V. Vedral, *Phys. Rev. Lett.* **119**, 240402 (2017).

ACKNOWLEDGMENTS

We thank O. Romero-Isart, L. Novotny, and T. Monteiro for insightful comments. U.D. and M.A. thank J. Ye for initially pointing out the relevance of coherent scattering to us. **Funding:** Supported by the European Research Council (ERC CoG QLev4G), the ERA-NET program QuantERA, QuaSeRT (project no. 11299191 via the EC, the Austrian ministries BMDW and BMBWF, and research promotion agency FFG), the Austrian Science Fund (FWF, project TheLO, Y 952-N36, START) and the doctoral school CoQuS (project W1210), and the research platform TURIS at the University of Vienna. **Author**

contributions: U.D., V.V., N.K., and M.A. conceived the experiment; U.D., M.R., and K.D. built the experiment (with initial contributions from D.G.) and performed the measurements; U.D. and D.G. performed the data analysis; and all authors were involved in writing and editing the paper. **Competing interests:** The authors declare no competing interests. **Data and materials availability:** All data needed to

evaluate the conclusions in the paper are present in the paper or the supplementary materials.

SUPPLEMENTARY MATERIALS

science.sciencemag.org/content/367/6480/892/suppl/DC1
Supplementary Text

Figs. S1 to S7
References (34–57)

29 November 2019; accepted 21 January 2020
Published online 30 January 2020
[10.1126/science.aba3993](https://doi.org/10.1126/science.aba3993)